Model-consistent universal wall-functions for RANS turbulence modelling

T. Knopp

Institute of Aerodynamics and Flow Technology
DLR (German Aerospace Center)
Bunsenstr. 10, 37073 Göttingen, Germany
Tobias.Knopp@dlr.de

1. Introduction

This paper is dedicated to *turbulence-model consistent universal wall-functions* for aerodynamic flows with separation, which allow for a considerable solver accelaration and reduction of memory consumptions at only a small loss in accuracy even in flows with separation and reattachment. A major concern in industrial CFD are still the huge computing costs for 3D flow simulations in complex geometries, in particular for unsteady calculations. Moreover, the increasing usage of CFD-solvers as part of optimization processes requires fast CFD-solutions. Wall-functions use near-wall modelling thereby avoiding the resolution of the strong gradients of the solution very close to the wall, and the number of boundary-layer nodes and the numerical stiffness can be reduced significantly.
The major short-coming of standard wall-functions, being based on the log-law, is that the underlying grid requirement $y^+(1) > 50$ ceases to be valid inevitably in flows with separation, as $y^+(1)$ goes to zero at the separation point and becomes small in regions of separated flow. Therein, denote $y^+(1) = y(1)u_\tau/\nu$ the distance of the first node above the wall in viscous length-scales, where $y(1)$ is the wall distance, u_τ is the friction velocity and ν is the viscosity. Historically, the first improvement over standard wall-functions was to use a so-called *hybrid* formulation, which are approximative velocity profiles for the entire near-wall region down to the wall. Hybrid wall functions are algebraic models (e.g. the model by Spalding) for the near-wall region ad hoc patched with the one- resp. two-equation turbulence model for the global (outer) flow. This turbulence model inconsistency causes a grid (i.e., $y^+(1)$)-dependent spreading of the solution, in particular for c_p and c_f.
This grid-dependence is one major reason for poor predictions of flows with separation. An initially high-Re grid with $y^+(1) \approx 50$ remote from the separation point becomes more and more a low-Re grid when approaching separation. Each change in $y^+(1)$ gives a small modelling error, which is accumulated and thus may lead to poor predictions near separation and reattachment.
Hence the second crucial modification was to devise universal wall-functions which are *consistent* with the turbulence model of the global (outer) flow, as revealed first by [1]. Such wall-functions are based on the universality of the near-wall RANS solutions for each given one- resp. two-equation model in zero-pressure gradient (ZPG) turbulent boundary layer flows. However, for successful application to non-equilibrium flow situations appearing in aerodynamic flows, the boundary treatment of the turbulence quantities deserves special attention [2].
This paper is organized as follows: Section 2. gives the governing equations for compressible fluid flow and RANS turbulence modelling. Section 3. describes the wall-function method. In Section 4. the method is applied to a boundary layer flow at zero-pressure gradient and to 2D airfoil flows with separation.

2. RANS equations for turbulent compressible flow

We consider the steady-state Favre-averaged compressible Navier-Stokes equations in a bounded Lipschitz domain $\Omega \subset \mathbb{R}^d$ $(d = 2, 3)$ with the eddy-viscosity assumption for the Reynolds-stress tensor and

the gradient-diffusion approximation for the turbulent heat-flux vector in conservative form

$$-\int_{\partial V} \mathbb{F}\cdot\vec{n}\,dS \;+\; \int_{\partial V} \mathbb{F}_v\cdot\vec{n}dS \;=\; 0$$

where V is an arbitrary control volume with closed boundary surface ∂V, and $\vec{n}$ is the unit normal vector in outward direction. The vector of conservative variables $\vec{W}$, and the convective and viscous flux tensor $\mathbb{F}$ and $\mathbb{F}_v$ resp. are given by

$$\vec{W} \;=\; \begin{pmatrix}\rho\\ \rho\vec{u}\\ \rho E\end{pmatrix}\,, \quad \mathbb{F} \;=\; \begin{pmatrix}\rho\vec{u}\\ \rho\vec{u}\otimes\vec{u}\;+\;p\mathbb{I}\\ \rho E\vec{u}+p\vec{u}\end{pmatrix}\,, \quad \mathbb{F}_v \;=\; \begin{pmatrix}0\\ \mathbb{T}\\ \mathbb{T}\,\vec{u}-\vec{q}\end{pmatrix} \tag{1}$$

where $E = c_v\theta + \vec{u}^2/2$ is the total specific energy. The pressure is given by $p = (\gamma-1)\rho(E-\frac{1}{2}\vec{u}^2)$. Strain rate tensor $\mathbb{T}(\vec{u})$ and heat-flux vector $\vec{q}$ are given by

$$\mathbb{T}(\vec{u}) \equiv \mathbb{S}(\vec{u}) - \frac{1}{3}\vec{\nabla}\cdot\vec{u}\,\mathbb{I}\,, \qquad \text{with} \quad \mathbb{S}(\vec{u}) = \frac{1}{2}\left(\vec{\nabla}\vec{u} + (\vec{\nabla}\vec{u})^T\right)\,, \quad \vec{q} = -\kappa_e\vec{\nabla}\theta$$

with effective viscosity $\mu_{\rm e} = \mu + \mu_{\rm t}$ and effective thermal conductivity $\kappa_{\rm e} = \kappa + \kappa_{\rm t}$. The turbulent viscosity μ_t is computed using a turbulence model of Spalart-Allmaras type [3] or of k-ω type [4] and for $\kappa_{\rm t}$ the concept of a turbulent Prandtl number is used.
In order to remedy the numerical problems associated with the no-slip boundary condition, we prescribe no-penetration and the tangential component of the wall-shear stress at solid walls, where we use the approximative relation

$$\mathbb{T}\cdot\vec{n} \;=\; (\mathbb{I}-\vec{n}\otimes\vec{n})\,\mathbb{T}\cdot\vec{n} + \vec{n}\otimes\vec{n}\,\mathbb{T}\cdot\vec{n} \;\approx -\tau_{\rm w}\vec{v}_{{\rm t},\delta}, \tag{2}$$

where $\vec{v}_{{\rm t},\delta}$ is the wall-tangential component of the velocity vector at the first node above the wall located at the matching boundary Γ_δ, and $\tau_{\rm w}$ is the magnitude of the wall-shear stress which is computed using a wall-function method, which is described in the next section.

3. Turbulence-model consistent universal wall-functions for RANS turbulence modelling

Wall-functions are based on the assumption that the near-wall flow between the wall and Γ_δ is described by the one-dimensional boundary layer equation. It is well-known that for equilibrium boundary layers, e.g., the flow over a flat plate at zero pressure gradient (ZPG), in the region between the wall and the outer edge of the logarithmic layer, the profiles for mean flow u and turbulence quantities k, ω, $\tilde{\nu}$ and hence ν_t are universal, i.e., they collapse when scaled with friction velocity u_τ and viscosity $\nu = \mu/\rho$

$$u^+ = \frac{u}{u_\tau}\,, \quad y^+ = \frac{yu_\tau}{\nu}\,, \quad \nu_{\rm t}^+ = \frac{\nu_{\rm t}}{\nu}\,, \quad p^+ = \frac{\nu}{\rho u_\tau^3}\frac{{\rm d}p}{{\rm d}x}\,, \quad k^+ = \frac{k}{u_\tau^2}\,, \quad \omega^+ = \frac{\omega\nu}{u_\tau^2}$$

A universal wall-function method is called *consistent* w.r.t. the specific turbulence model used for the global flow, if the low-Re RANS solution for a flat-plate zero-pressure gradient boundary layer flow also solves the 1D boundary layer equation which determines the wall-function solutions, viz.,

$$(1+\nu_{\rm t}^{\rm bl,+})\frac{{\rm d}u^{\rm bl,+}}{{\rm d}y^+} \;=\; 1 \qquad \text{in} \quad (0, y_\delta^+) \tag{3}$$

This implies $\nu_t^{\rm bl} = \nu_t$, i.e., wall functions have to be turbulence-model specific, as revealed by [1]. Consistency ensures that $u = u^{bl}$ in the entire near-wall region Ω_δ. Then predictions for surface transfer coefficients like $c_{\rm p}$, $c_{\rm f}$ are independent of the location of the matching boundary Γ_δ. In contrast, the grid-dependent spreading of standard hybrid wall-functions is shown in in Figure 4 (right).

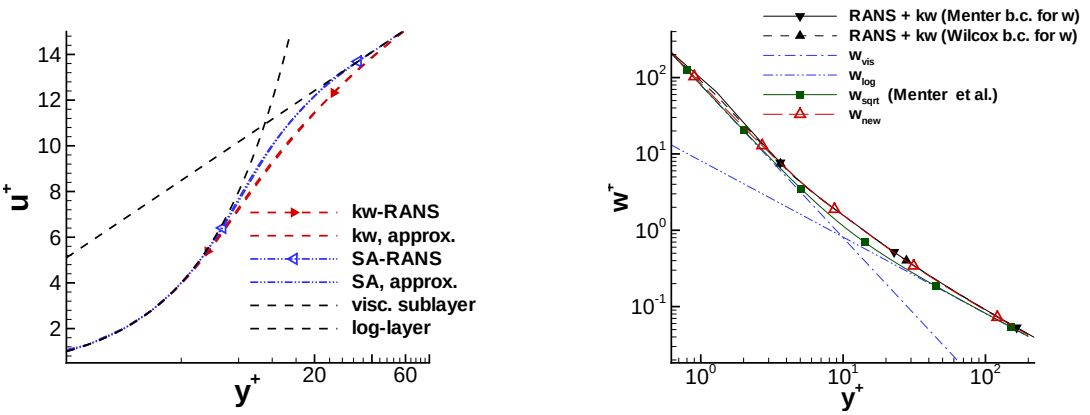

Figure 1: Model-consistent universal wall-functions for SA- and k-ω model (left) and proposal (10) for a new wall-law for the turbulence frequency ω in the k-ω turbulence model (right).

3..1. New proposal for closed-form turbulence model specific wall functions

As the near-wall profiles of different versions of the Spalart-Allmaras model resp. the k-ω model in zero-pressure gradient (ZPG) boundary layer almost collaps, see [2], it is sufficient to determine one model-consistent universal wall-function for the Spalart-Allmaras model and one for the k-ω model. These may be viewed as an interpolation of the ZPG RANS solutions using a combination of two suitable solution-fitted basis functions, viz., the wall-law by Spalding and the law by Reichardt

$$\mathrm{F}_{\mathrm{SA,a}} = (1-\phi_{\mathrm{SA}})\mathrm{F}_{\mathrm{Sp},5} + \phi_{\mathrm{SA}}\mathrm{F}_{\mathrm{Rei,m}}, \quad \phi_{\mathrm{SA}} = \tanh(\mathrm{arg}^3), \quad \mathrm{arg} = y^+/24 \tag{4}$$

$$\mathrm{F}_{k\omega,\mathrm{a}} = (1-\phi_{k\omega})\mathrm{F}_{\mathrm{Sp},3} + \phi_{k\omega}\mathrm{F}_{\mathrm{Rei,m}}, \quad \phi_{k\omega} = \tanh(\mathrm{arg}^2), \quad \mathrm{arg} = y^+/50 \tag{5}$$

which are plotted in Figure 1 (left). Therein, we use Reichardt's law of the wall

$$u^+ = \mathrm{F}_{\mathrm{Rei}}(y^+)\,, \qquad \mathrm{F}_{\mathrm{Rei}}(y^+) \equiv \frac{\ln(1+0.4y^+)}{\kappa} + 7.8\left(1 - e^{-\frac{y^+}{11.0}} - \frac{y^+}{11.0}e^{-\frac{y^+}{3.0}}\right). \tag{6}$$

and use the fact that Reichardt's law blended with the classical log-law $\mathrm{F}_{\mathrm{log}} = \ln(y^+)/\kappa + 5.1$ gives an excellent agreement in the log-layer when using the formula

$$\mathrm{F}_{\mathrm{Rei,m}} = (1-\phi_{\mathrm{b1}})\mathrm{F}_{\mathrm{Rei}} + \phi_{\mathrm{b1}}\mathrm{F}_{\mathrm{log}}\,, \quad \phi_{\mathrm{b1}} = \tanh(\mathrm{arg}^4)\,, \quad \mathrm{arg} = y^+/27. \tag{7}$$

Spaldings law with parameter $N \in \{\,3,4,5\,\}$ is given by the inverse formula

$$y^+ = F^{-1}_{\mathrm{Sp,N}}(u^+)\,, \qquad F^{-1}_{\mathrm{Sp,N}}(u^+) \equiv u^+ + e^{-\kappa\,5.2}\left(e^{\kappa u^+} - \sum_{n=0}^{N}\frac{(\kappa u^+)^n}{n!}\right). \tag{8}$$

Then given $\vec{u}$ on Γ_δ from the global RANS solution of the previous iteration cycle and denoting u_δ the magnitude of the wall-parallel velocity at Γ_δ, the matching condition $u^{\mathrm{bl}} = u_\delta$ on Γ_δ and $u^{\mathrm{bl}} = u_\tau \mathrm{F}(yu_\tau/\nu)$ imply

$$\mathrm{F}\left(\frac{y_\delta u_\tau}{\nu}\right) = \frac{u_\delta}{u_\tau} \quad \text{resp.} \quad \mathrm{F}^{-1}\left(\frac{u_\delta}{u_\tau}\right) = \frac{y_\delta u_\tau}{\nu} \tag{9}$$

which can be solved for u_τ using Newton's method. Then we set $\tau_w^{\mathrm{bl}} = \rho u_\tau^2$ to be imposed as wall boundary condition for the global RANS problem (2) in the next iteration step.
Moreover, for ω appearing the k-ω model the following wall-function is proposed, see Figure 1 (right)

$$\omega = \phi\omega_{\mathrm{b1}} + (1-\phi)\omega_{\mathrm{b2}}, \quad \phi = \tanh(\mathrm{arg}^4), \quad \mathrm{arg} = \frac{y^+}{10} \tag{10}$$

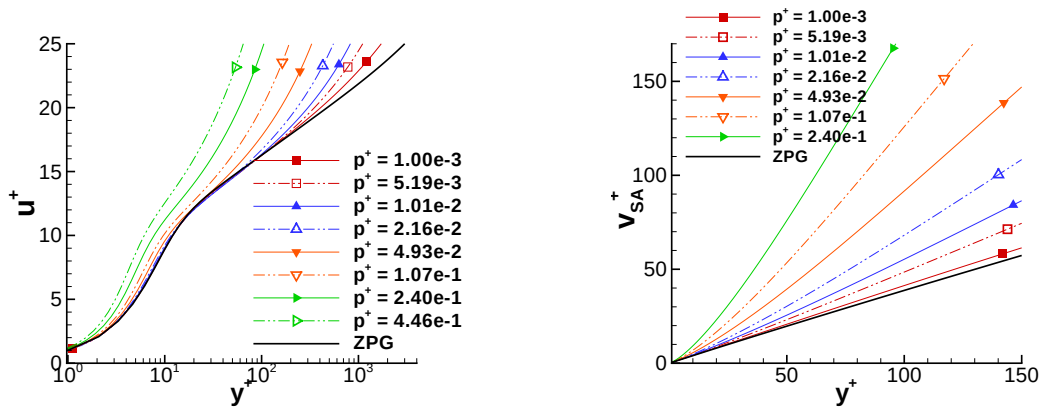

Figure 2: Profiles for u^+ and $\tilde{\nu}^+$ for SA-E model at different p^+-stations for the APG flow [1].

where we use the following blending formula and the asymptotic relations

$$\omega_{\rm b1} = \omega_{\rm vis} + \omega_{\rm log}\,, \quad \omega_{\rm b2} = \left(\omega_{\rm vis}^{1.2} + \omega_{\rm log}^{1.2}\right)^{1/1.2}, \quad \omega_{\rm vis} = \frac{6\nu}{\beta_\omega y^2}\,, \quad \omega_{\rm log} = \frac{u_\tau}{\sqrt{\beta_k}\kappa y}.$$

with constants β_k, β_ω stemming from the transport equation for ω

$$\vec{\nabla}\cdot(\rho\vec{u}\omega) - \vec{\nabla}\cdot\left((\mu + \sigma_\omega\mu_{\rm t})\,\vec{\nabla}\omega\right) \;=\; 2\gamma\rho\;\mathbb{T}(\vec{u}) : \vec{\nabla}\vec{u} - \beta_\omega\rho\omega^2 \tag{11}$$

3..2. Near-wall behaviour of turbulence quantities in non-equilibrium flow situations

The aim is to apply wall-functions to aerodynamics flows which are characterised by a locally large departure from the assumption of equilibrium flow. Then the term p^+ in the original right hand side $1+p^+$ of (3) causes a departure from the universal profiles which becomes more pronounced as p^+ increases. We consider the boundary layer flow with adverse pressure gradient devised by [1]. A detailed discussion can be found in [2]. The flat plate has length $L = 9\text{m}$, $u_\infty = 78\text{ms}^{-1}$ and $\nu_\infty = 1.5\times10^{-5}\text{m}^2\text{s}^{-1}$ At distance $y = 0.5\text{m}$, suction and blowing is imposed by prescribing the wall-normal velocity component $v(x) = A\exp(-b(x-x_\alpha)^2) - A\exp(-b(x-x_\beta)^2)$ with $x_\alpha = 2.5$, $x_\beta = 5.5$, $A = 0.35x$, $b = 108/6^2$. which produces a streamwise pressure gradient leading to separation.

For the SA-E model, the region occupied by the universal ZPG solution in reduced progressively, see Figure 2 (left), whereas $\tilde{\nu}^+$ shows a much larger deviation from the universal ZPG solution than would be expected from the behaviour of the u^+-profiles, see Figure 2 (right). Figure 3 shows the profiles for k^+ and ω^+. For ω a progressive reduction of the region of validity of the universal ZPG solution is observed, whereas for k a general breakdown of the ZPG solution in the *entire* near-wall region can be seen. This causes the general breakdown of the universal ZPG solution for u^+ for the SST k-ω model, see Figure 4 (left).

From these results, the following implications for the near-wall treatment of the turbulence quantities may be drawn. From Figure 3 (right) we see that prescribing ω also at Γ_δ does not lead to a model-inconsistency for large p^+-values at least for $y^+(1) < 10$. On the other hand, k and $\tilde{\nu}$ exhibit a large departure from the universal solution in the entire near-wall region. Therefore off-wall boundary conditions, i.e., prescribing k and $\tilde{\nu}$ on Γ_δ based on the ZPG profile, are avoided. Instead homogeneous Dirichlet conditions are imposed on $\Gamma_{\rm w}$. Finally, regarding the boundary condition of ω, we mention that two treatments are popular in CFD solvers, viz., $\omega = \omega_\delta$ on Γ_δ with $\omega_\delta = 6\nu/(\beta_\omega y_\delta^2)$ (Wilcox b.c.) and *(ii)* $\omega = 10\;\omega_\delta$ on $\Gamma_{\rm w}$ (Menter b.c.). We remark that Wilcox b.c. was found to be significantly superior in giving grid-independent wall function results, see [2] for more details.

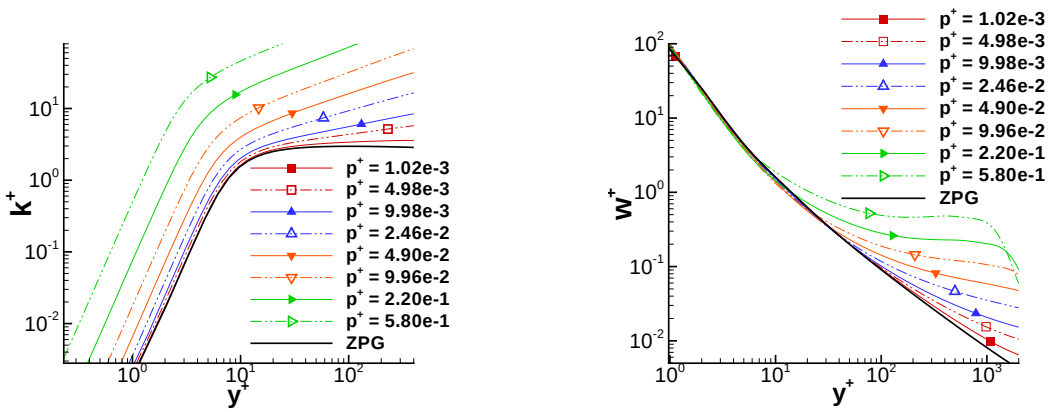

Figure 3: Near-wall profiles for k^+ and ω^+ for SST k-ω model at different p^+-stations for APG flow [1].

4. Numerical results

4..1. Numerical method

The numerical results are obtained using the DLR TAU-code, which is an unstructured finite-volume solver of cell-vertex type. A central scheme with artificial scalar dissipation is used for the inviscid fluxes. The arising fixed-point problem is iterated in fictitious pseudo-time using a low-storage k-stage Runge-Kutta scheme by Jameson, see also [2] and references therein.

4..2. Flat plate turbulent boundary layer at zero pressure gradient

The ability of the new wall function proposal to give solutions almost independent of the wall-normal grid spacing is studied for the boundary layer flow at zero pressure gradient (ZPG) Flow 1400 [5] with $u_\infty = 33\mathrm{ms}^{-1}$, $\nu = 1.51 \times 10^{-5}\mathrm{m}^2\mathrm{s}^{-1}$ and the lenght of the plate is $l = 5\mathrm{m}$. Figure (4) (right) shows the relatively large deviation from the low-Re solution for inconsistent wall-functions if $y^+(1) \in (5, 25)$. Figures 5-6 show the almost grid independent predictions for $C_f(x)$ and $u^+(y^+)$ for the SA-Edwards

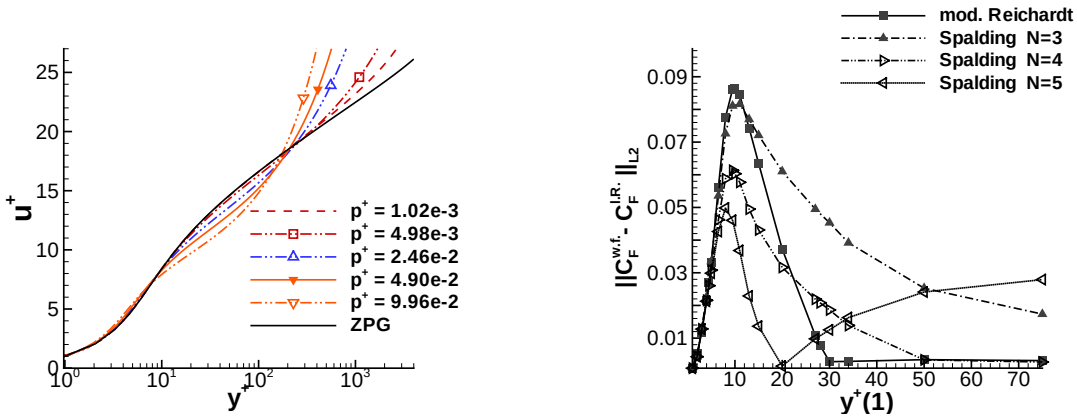

Figure 4: Left: Near-wall u^+-profiles for SST k-ω model for APG flow [1]. Right: Grid-dependent predictions using inconsistent classical hybrid wall laws for SA-Edwards model.

(SA-E) model and for the Menter baseline k-ω model [4].

4..3. Application to airfoil flows

First we apply the method to the transonic airfoil flow RAE-2822 case 10 with shock induced separation at $Ma = 0.75$, $Re = 6.2 \times 10^6$ and $\alpha = 2.8^\circ$ studied experimentally in [6]. We use a series of grids of

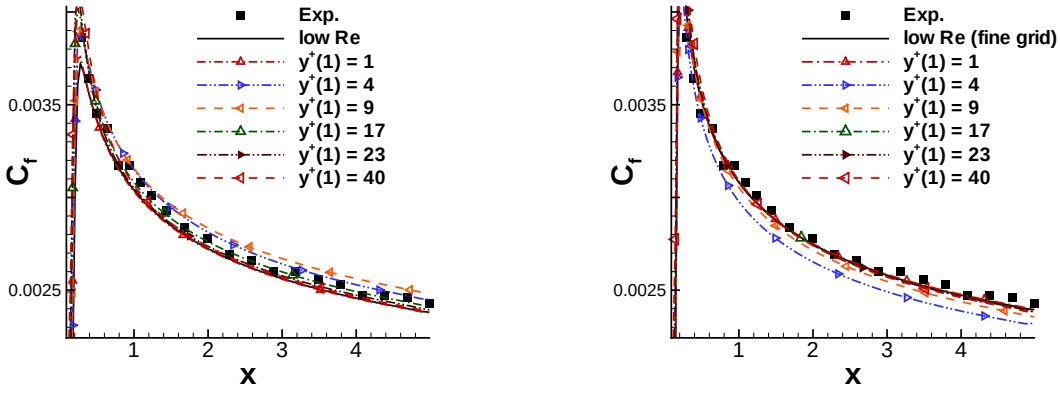

Figure 5: Almost grid-independent prediction of C_f for ZPG flow [5] using analytical model-consistent wall-function Eq. (4) for SAE model (left) and Eq. (5)) for Menter baseline model (right).

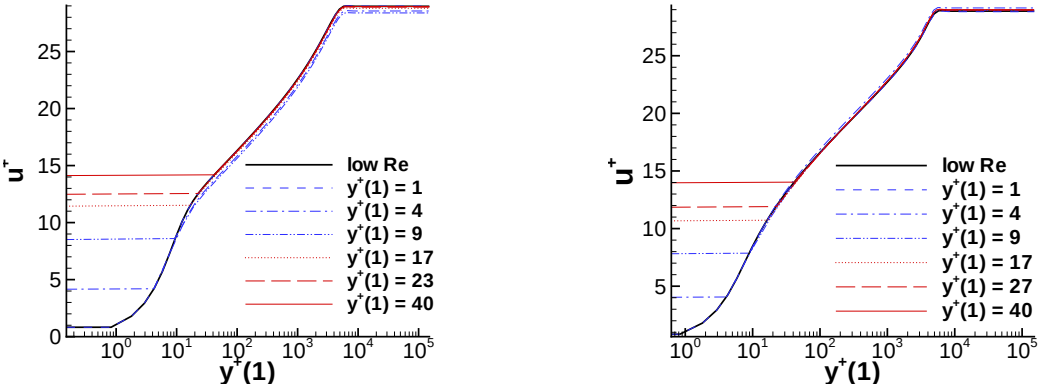

Figure 6: Velocity profiles for ZPG flow [5] for SA-E model (left) and Baseline k-ω model (right).

O-type with $y^+(1)$ varying from one to 60. Figures 7-8 show that for the SST k-ω model, the predictions for c_p and c_f are remarkably grid-independent, in particular regarding the shock position.
Secondly, the wall-function method is applied to the subsonic flow around the "A-airfoil" in highlift configuration at $Ma = 0.15$, $Re = 2.0 \times 10^6$, and $\alpha = 13.3°$, studied experimentally in [7]. In contrast to the experiment, the airfoil surface is treated here fully turbulent. On the upper side of the airfoil, the strong adverse pressure gradient causes the turbulent boundary layer to separate close to the trailing edge. The $y^+(1)$-distributions for the series of O-type grids are shown in Figure 9. For the SST k-ω model with Wilcox b.c., on all grids the agreement in c_f (and hence in the separation point) with the low-Re solution is remarkably good, in particular for $y^+(1) \lessapprox 10$, see Figure 10. Figure 11 shows details of the streamtraces in the recirculation region near the trailing edge for the SST model with results on the $y^+(1) = 40$-grid being close to the low-Re solution.

5. Conclusions

A turbulence model specific wall-function method for RANS turbulence modeling of SA- and k-ω type has been presented which uses a boundary treatment for the turbulence quantities which is motivated by an investigation of the near-wall solutions in non-equilibrium flow situations. This approach was demonstrated to give very promising results for airfoil flows with separation.

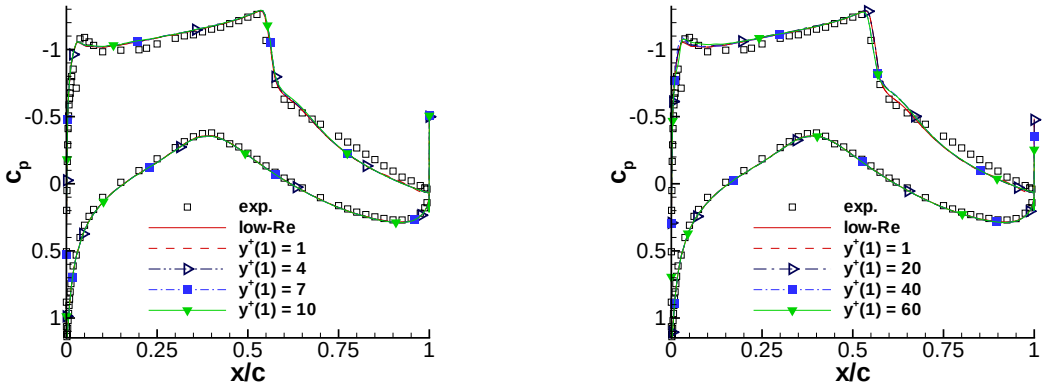

Figure 7: RAE case 10: Distribution of c_p for SST k-ω model with Wilcox b.c.

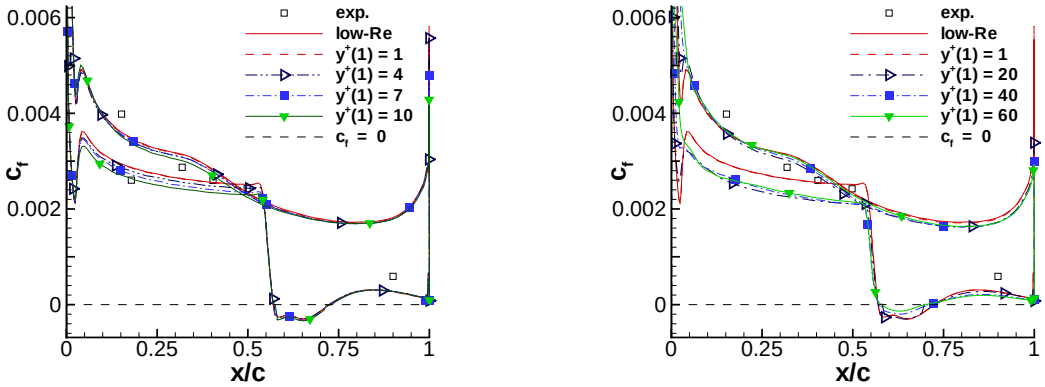

Figure 8: RAE case 10: Prediction of c_f for SST k-ω model with Wilcox b.c.

References

[1] G. Kalitzin, G. Medic, G. Iaccarino and P. Durbin, "Near-wall behaviour of RANS turbulence models and implications for wall functions", *Journal of Computational Physics*, **2**04, 265–291 (2005).

[2] T. Knopp, T. Alrutz and D. Schwamborn, "A grid and flow adaptive wall-function method for RANS turbulence modelling", *Journal of Computational Physics* (accepted).

[3] J.R. Edwards and S. Chandra, "Comparison of eddy viscosity-transport turbulence models for three-dimensional, shock separated flowfields", *AIAA Journal*, **3**4, 756–763 (1996).

[4] F.R. Menter, "Zonal two equation k/ω turbulence models for aerodynamic flows", *AIAA Paper 1993-2906*, (1993).

[5] D. E. Coles and E. A. Hirst (Eds.), *Computation of Turbulent Boundary Layers - 1968 AFOSR-IFP-Stanford Conference*, Stanford, (1969).

[6] P. H. Cook, M. A. McDonald and M.C.P. Firmin, "Aerofoil RAE 2822 - Pressure distributions and boundary layer and wake measurements", *AGARD Advisory Report AR-138*, A6.1-A6.77, (1979).

[7] Ch. Gleyzes, "Opération décrochage - Résultats des essais à la soufflerie F2", *RT-DERAT 55/4004 DN, ONERA*, (1988).

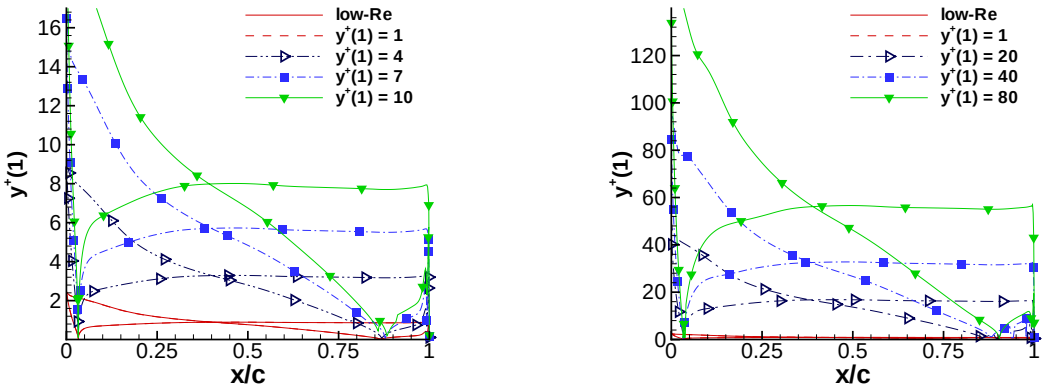

Figure 9: A-airfoil: Distribution of $y^+(1)$ for the SST k-ω model.

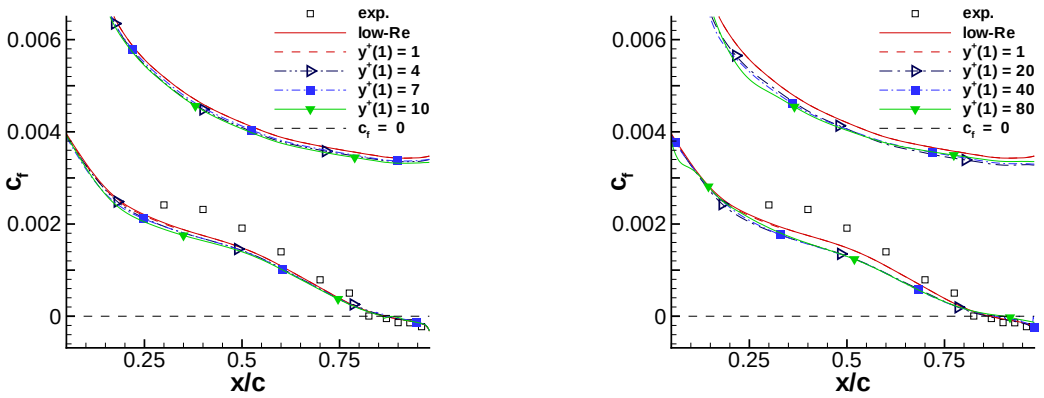

Figure 10: A-airfoil: Prediction for c_{f} for SST k-ω model with Wilcox b.c.

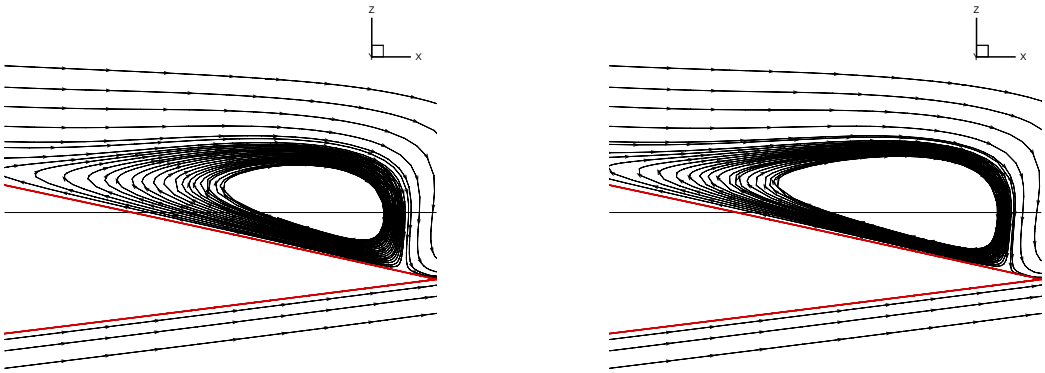

Figure 11: A-airfoil: Details of the separation region on a wall-resolved grid with $y^+(1) = 1$ (left) and using wall-functions on a grid with $y^+(1) = 40$ (right).